Improved Method for
Arc Flash Hazard Analysis

R. Wilkins, M. Allison and M. Lang
May 2004

Improved Method for Arc Flash Hazard Analysis

R. Wilkins, M.Allison and M. Lang

Ferraz Shawmut, Inc.

Newburyport, USA

May, 2004

bobwilkins@clara.co.uk , malcolm.allison@ferrazshawmut.com , mike.lang@ferrazshawmut.com

Abstract - **Conventional arc flash hazard calculators use simple formulae to calculate the flash protection boundary and the incident energy density, but these methods do not represent the effects of the power supply system correctly. A new method is described which models the transient response of a 3-phase power system and its interaction with an arcing fault. The operation of current-limiting fuses in the time domain, and the focusing effect of the equipment enclosure are also considered.**

Keywords - arc flash hazard, current-limiting fuses

I.   INTRODUCTION

The 2002 edition of the NEC requires equipment, on which work may be required to be done when energized, to be labeled, warning of arc flash hazard [1-3]. The draft 2004 edition of NFPA 70E requires a flash hazard analysis to be done before a person can work near to energized equipment, and to determine the type of protective clothing needed [2].

There are several different methods in use at present to calculate the flash boundary distance and incident energy upon a worker [2,4-7], and the IEEE standard 1584 contains formulae based on a statistical fit to test data obtained in several high-power test laboratories in North America [8].

In this paper, an improved method which uses time-domain analysis is presented. It can be used as an arc flash calculator, but it also allows current limitation by fuses and other effects to be studied.
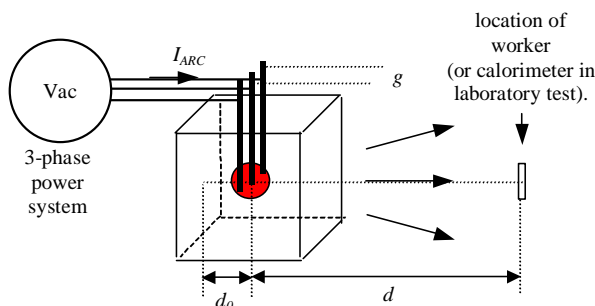

Figure 1.   Arc flash in an open box

Fig. 1 shows a schematic representation of the test set-up which was used in most of the IEEE tests to model an arc flash hazard incident, the arcing being initiated by fine trigger fuse wires. High-current arcs which are not restricted move, due to magnetic forces, to increase the area of the circuit loop. For the geometry shown this causes the arcs to be driven downwards and to burn from the electrode (busbar) tips. However the behavior of the 3-phase free-burning arcing fault in equipment is chaotic, involving rapid and irregular changes in arc

geometry due to thermal buoyancy (convection) and electromagnetic forces, arc extinction, plasma jets, sudden shortening due to restriking and reconnection across electrodes or plasma parts, and many other effects.

These effects have been vividly illustrated by Stokes and Sweeting [9] using high-speed video photography. For tests in the open, they showed the formation of an expanding plasma cloud, fed by jets from the electrodes, and forced away from the electrodes (downwards in the case of Fig. 1).

The calorimeters shown in Fig 1, which represents the IEEE tests, are not directly located in the path of the plasma cloud, and receive heat energy from the arcing zone principally in the form of radiation.

II.   THE IEEE 1584 FORMULAE

There are two principal stages in arc flash calculations:

(a) calculation of the r.m.s. arcing current I_{ARC} so that the operating time of protective devices can be found

(b) calculation of the incident energy density E at a distance d so that a safe working distance or the required personal protective equipment can be determined.

In IEEE 1548 the following equation is given for the calculation of I_{ARC} (originally for system voltages under 1kV).

$$\log_{10} I_{ARC} = K_A + 0.662 \log_{10} I_{BF} + 0.0966V + 0.000526g$$
$$+ 0.5588V \log_{10} I_{BF} - 0.00304\, g \log_{10} I_{BF} \qquad (1)$$

where
K_A = -0.153 or -0.097 (open or box configuration)
I_{BF} = bolted 3-phase symmetrical fault current, kA
V = system voltage, kV
g = gap between arcing electrodes , mm.

Equation (1) was derived using a least-squares method, to obtain a good fit to the test data. However, the grouping of the variables on the right-hand-side of (1) is not based on physical phenomena, and can produce anomalous results.

In reality the resistance of the arcing fault produces an arcing current which must always be lower than the bolted fault current. Furthermore if the arcing gap distance is increased, the resistance increases (although by a relatively small amount [9]), and the arcing current should fall.

Fig. 2 shows the ratio of arcing current to bolted fault current for the "box" case, with V = 0.48kV, and arcing gaps from 32 to 152mm. The ratio should always be less than 1.0, but Fig. 2 shows that it can exceed 1.0 for low bolted fault currents.
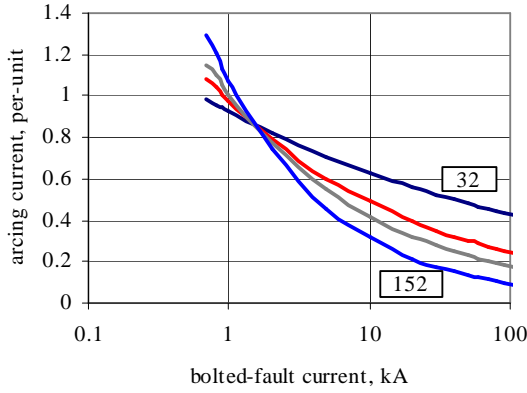
Figure 2. I_{ARC}/I_{BF} calculated from equation (1).

Furthermore, for bolted fault currents less than 1.489kA, irrespective of system voltage, the effect of the gap length is reversed (incorrectly), giving higher arcing currents for longer gaps. Although at 0.48kV the situation improves for bolted fault currents above 1.489kA, the effect of the anomaly is still significant for much higher values. Other anomalies occur at higher voltages. For example, if $V > 0.783$ kV and $g=32$mm, the arcing current exceeds I_{BF} at $I_{BF} = 100$kA.

For higher voltage systems the IEEE 1584 equation is

$$\log_{10} I_{ARC} = 0.00402 + 0.983 \log_{10} I_{BF} \qquad (2)$$

This gives arcing currents higher than the bolted fault current for $I_{BF} < 1.724$kA.

The second stage of the IEEE 1584 method requires the calculation of a normalized incident energy density E_n using

$$\log_{10} E_n = K_1 + K_2 + 1.081 \log_{10} I_{ARC} + 0.0011g \qquad (3)$$

where K_1 = -0.792 or -0.555 (open or box configuration)
K_2 = 0 or -0.113 (grounded or ungrounded system)

This is then adjusted to the actual fault duration (linearly) and for the distance d using a power-law with a "distance exponent" X, which depends on the equipment type. Equation (3) can also give anomalous results. The test results with the electrodes arranged as in Fig. 1 show that the incident energy is significantly higher for tests in a box, because of the "focusing" effect, but equation (3) can produce the opposite result, as shown in Fig. 3.

The curves in Fig. 3 were calculated using the "switchgear" distance exponents given in [8] (1.473 for LV and 0.973 for HV), and the results shown are independent of the actual voltage, gap length and bolted fault current. Using the LV equations the "open" incident energy density exceeds the "box" value if d is less than 166mm, while for the HV equations, this occurs at 358mm, but the effect of the anomaly remains significant for higher values of d.

The reason for the anomaly lies in the use of different distance exponents. The normalized incident energy E_n(box) is higher than E_n(open) at the standard distance of 610mm [8], but when this is corrected for lower values of d the situation can be reversed, because the correction curve for E_n(open) with $X=2$ rises more steeply than for E_n(box).
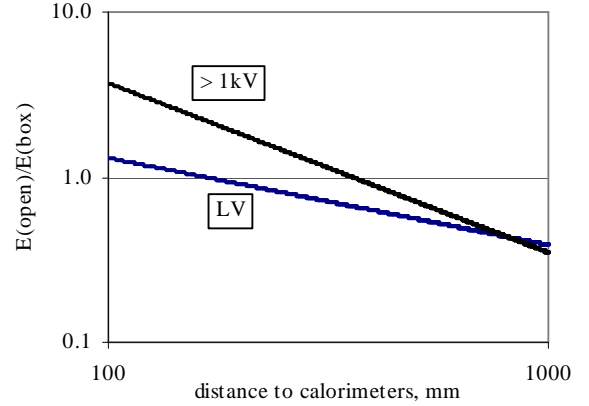

Figure 3.   Incident energy ratio using IEEE 1584 equations

III.   TIME DOMAIN MODEL

The anomaly in the calculation of I_{ARC} can be avoided by the use of a time-domain model such as that shown in Fig. 4. The circuit parameters are derived from the system data (voltage, bolted-fault current, frequency, X/R ratio and closing angle).

Although the fault arc behavior is difficult to model, the behavior of the electrical circuit can be computed precisely, reducing the area of uncertainty to that of the fault arc model. Whatever fault arc model is used, the calculated arcing current will always be lower than the bolted fault current with a time domain model of this type.
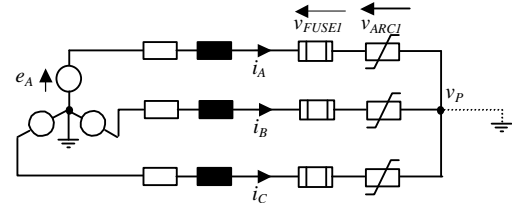

Figure 4.   Circuit model

The circuit model in Fig. 4 includes a set of three current-limiting fuses in series with the arcing fault. The arcing fault is initially modeled as a set of fine trigger fuse wires with a fixed melting I²t, and then the subsequent 3-phase arcs are modeled as a star-connected set of non-linear resistances. The transient circuit current can then be found by numerical solution of the circuit differential equations:

$$\frac{di_A}{dt} = \frac{e_A - R\,i_A - v_{FUSE1} - v_{ARC1} - v_P}{L}$$
$$\frac{di_B}{dt} = \frac{e_B - R\,i_B - v_{FUSE2} - v_{ARC2} - v_P}{L} \qquad (4)$$
$$\frac{di_C}{dt} = \frac{e_C - R\,i_C - v_{FUSE3} - v_{ARC3} - v_P}{L}$$

If the fictitious star point is grounded $v_P = 0$ and the computed phase currents do not interact. In this case computation continues until all fuses have cleared or until a preset time is reached, corresponding to the opening of a backup breaker. However an ungrounded model is more realistic. For this case the sum of the phase currents is zero, which enables the instantaneous potential v_P to be calculated as follows:

(a) if no fuses have cleared

$$v_P = - (v_{FUSE1} + v_{FUSE2} + v_{FUSE3} + v_{ARC1} + v_{ARC2} + v_{ARC3}) / 3$$

(b) after the first fuse has opened, say in phase a

$$v_P = (e_B + e_C - v_{FUSE2} - v_{FUSE3} - v_{ARC2} - v_{ARC3}) / 2$$

Cyclically similar expressions may be written if phase b or phase c clears first [11]. If fuses are not used, the fuse voltages are all set to zero.

IV. FAULT ARC CHARACTERISTICS

The single-phase high-current arc in air has a rising V-I characteristic which can be represented as

$$V_{ARC} = V_E + k I_{ARC}{}^X g^Y \qquad (5)$$

Measurements by Fisher [12] using currents up to 41.6kA and arcing gaps g from 25-100mm found that $X \approx 0.15$ and $Y \approx 0.5$. Ignatko [13] studied arcs from 5-150kA with gaps from 5-200mm. He measured the electrode-fall voltage (V_E) with Langmuir probes (23.5V for copper electrodes), and the actual arc length (which is greater than the gap distance) was measured photographically, to obtain the column gradient. Ignatko's data also fits the form of equation (5), with similar X and Y to Fisher's.

Stokes and Oppenlander [14] found $X \approx 0.12$ and $Y \approx 1.0$ for horizontal and vertical gaps of 5-500mm with currents up to 20kA. Their photographs revealed the complex variations in arc geometry in detail. Paukert [15] reviewed data from seven different laboratories and found approximate average values of $X \approx 0.2$ and $Y \approx 0.47$.

Given the very variable nature of the fault arc, the data in the literature shows a remarkable agreement. The arc voltage shows a weakly rising dependence on current, with $X \approx 0.12$-0.2. In some cases it is not clear whether published data refers to instantaneous current or true r.m.s. current, but the trend is the same. The dependence on g is more variable, probably as a result of the use of differing electrode geometries. For the 3-phase case with horizontal electrodes, Stokes and Sweeting [9] found $X \approx 0.12$ and a weak dependence upon gap distance.

As a first step (and as originally suggested by Fisher) the 3-phase case can be represented as three separate star-connected single-phase arcs (see Fig. 4), each of which can be modeled by an equation of the same form as (5).

For use with the 3-phase time domain model, the unknown values of X and Y were determined using the following procedure. First the value of a constant arc voltage was found which gave a true r.m.s. arcing current which agreed exactly with the values measured in the IEEE tests. This was done by repeatedly solving equation (4) for each test shot, computing the true r.m.s. current over the last cycle before the circuit opened, and iteratively adjusting V_{ARC} to obtain agreement. Then X and Y were determined by a multiple regression fit to equation (5). (304 test shots were used in the analysis - the tests with series current-limiting fuses being excluded). This gave $X = 0.173$ and $Y = 0.222$, values which are consistent with the literature.

Then it was assumed that the same X and Y can be used to relate the instantaneous arc voltage and current (v and i), giving a nonlinear transient arc model of the form

$$v_{ARC} = V_E + K i_{ARC}{}^{0.173} g^{0.222} \qquad (6)$$

Finally the value of K was found by a second iterative fitting to the measured arcing current. However K was not constant, but a relatively strong function of the line-to-line test voltage V_{LL}. ($K = 1.827 V_{LL}{}^{0.377}$ with V_{LL} in V). This dependency is not easy to explain, but it is also implied in Schau and Schade [16] and the IEEE formula. It is probably connected with the assumption that the arc is quasi-static, and possibly that the effects of arc extinction and restriking around voltage zero were not modeled. There was also a box effect; K must be multiplied by 0.797 for tests in a box.

Using this model together with the circuit equations (4), the circuit currents, voltages, power and energy can be computed. Typical results are shown in Figs. 5-8 for an ungrounded arcing fault.
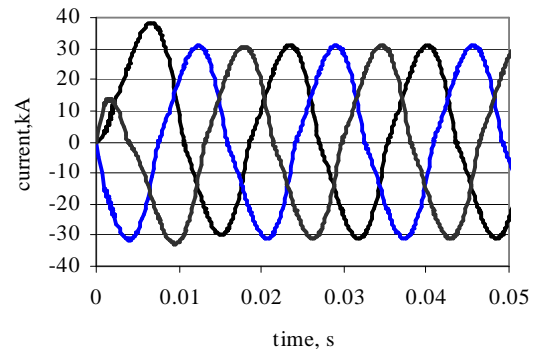
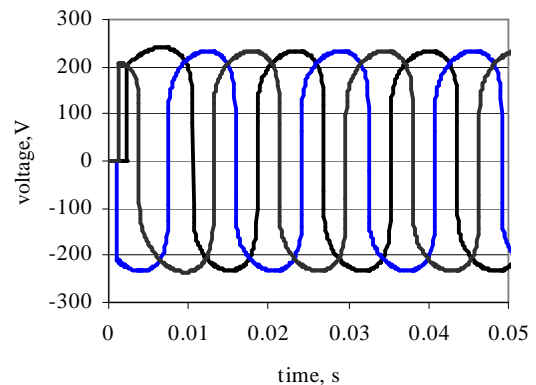Figure 5. Computed current transients

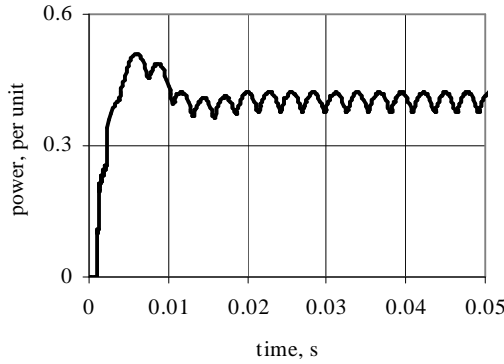Figure 6. Computed fault arc voltage transients

Figure 7.   Instantaneous 3-phase power

The waveshapes are similar to published data [5,16]. The current stabilizes quite quickly because of the damping effect of the fault arc resistance. The delay in appearance of the arc voltage is the fusion time of the fine trigger wires in each phase. Fig. 7 shows the instantaneous power as a fraction of the bolted-fault VA. The build-up of arc energy in Fig. 8 is almost linear, but with a delay of a few milliseconds after the fault begins.
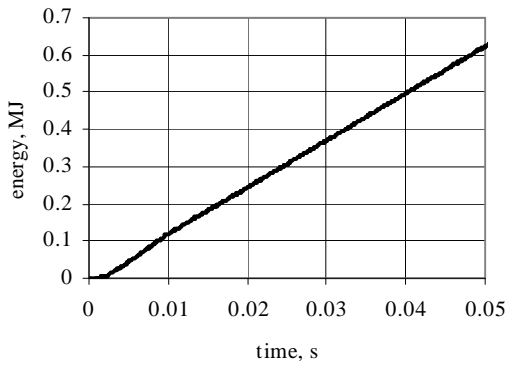

Figure 8.   Total arc energy

These solutions were obtained using 4th order Runge-Kutta integration of the equations, with automatic adjustment of the time step to achieve a preset accuracy. However the resistance of the arc model (6) tends to infinity as the current nears zero, giving a very low circuit time-constant, which causes the time step to be reduced to a very small value, and the solution "grinds to a halt". A numerical procedure for solving this problem, ensuring a smooth and rapid progression of the solution through the current zeros is given in [10].

Gammon and Matthews [17] calculated arcing currents for single-phase arcing faults using a similar time-domain method (Runge-Kutta integration, using both Fisher's and Stokes and Oppenlander's model). They assumed that the arc extinguishes at each current zero and then reignites in the next half-cycle when the gap voltage reaches a fixed breakdown level (dielectric reignition), whereas the model described here shows a continuous variation of current through the zero-crossing period. Dielectric reignition can be seen to occur for a single-phase arc where the power input to the plasma drops to zero when the current reaches zero. However for a 3-phase arcing fault the situation is less clear. Although the current in one phase may reach zero the power input to the plasma continues via the other two phases [9].

Using the time-domain model the r.m.s. arcing current (geometric mean value for the 3 phases over the last cycle before circuit opening) was computed and compared with the measured values given in [8]. The results are shown in Fig. 9, and the values predicted by the IEEE equation (1) are shown in Fig 10.
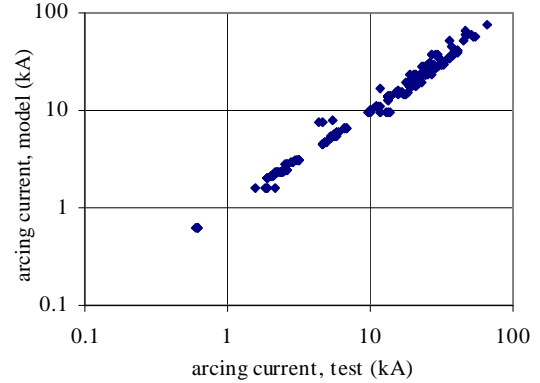

Figure 9.   Comparison of predicted and measured arcing current (time-domain model).
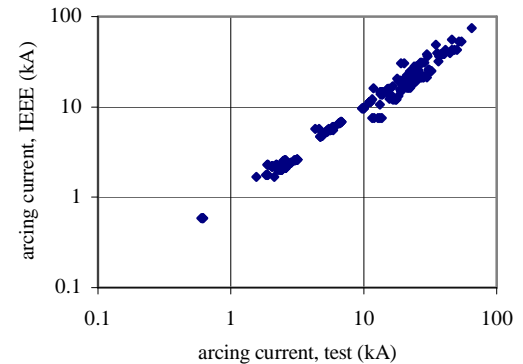

Figure 10. Comparison of predicted and measured arcing current (IEEE 1584 model).

Fuses were not used for the test data of Figs. 9 and 10, the circuit being cleared by a back-up breaker. The data covers voltages from 208V to 13.8kV, bolted fault currents from 700A to 106kA, arcing gaps from 7.1mm to 152mm, and various box dimensions, as well as tests in the open (304 tests in all). The time-domain model gives a slightly better correlation (r^2=0.989) than the IEEE equation (r^2=0.978). However this small improvement is not its main advantage. The time domain model always predicts arcing currents which are lower than the bolted fault current, and which fall as the gap length increases.

V.   CALCULATION OF INCIDENT ENERGY DENSITY

The electrical energy input to the high-current arc plasma is transferred to the surroundings by conduction, convection and radiation, and is also consumed in melting and vaporizing the electrode metal at the arc roots. For enclosed equipment a

substantial part of the energy is also converted to pressure rise. The overall energy balance is discussed in [16].

For the geometry of Fig. 1 the calorimeters principally intercept radiant heat from the arcing zone. For tests in the open, with a total energy W_{ARC} the direct radiated energy density at a distance d is $\beta W_{ARC}/(4\pi d^2)$ where β is the fraction of the total arc energy which is emitted as radiant heat, assuming spherical symmetry. In this case the distance exponent is 2.

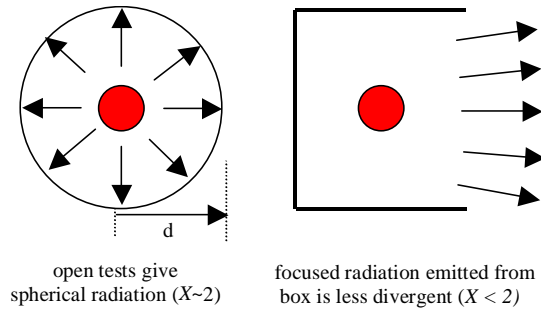For tests in an open box, the focusing effect of the box changes the situation, as shown in Fig. 11.

Figure 11. Box focusing effect

Reflections of radiant heat from the back and sides of the box can make the arc and the box appear as one much larger heat source, reducing the effective distance exponent.

A. Tests in the open

Fitting to the IEEE test data using multiple regression gave the following model :

$$E_{max} = 84.61\, E_S^{\,0.958}\, g^{\,0.284}\, V_{LL}^{\,-0.532} \qquad (7)$$

E_{max} = mean maximum energy density at a distance d, (cal/cm^2)

E_S = spherical component of energy density, (J/mm^2)
= $W_{ARC}/(4\pi d^2)$

W_{ARC} = total arc energy computed using the time domain model , J

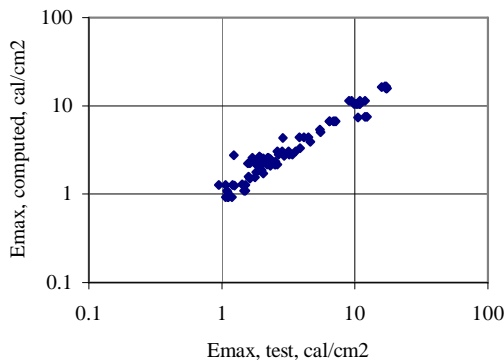Fig. 12 shows a good correlation ($r^2 = 0.949$) between the predictions of (7) and the test values.

Figure 12. Predicted incident energy density, all open tests

B. Tests in a box with one side open

To avoid the anomaly caused by the use of distance exponents less than 2, it is possible to calculate the focusing effect of the box directly, using radiative view factors [10,18]. The view factor F_{ij} between 2 surfaces i and j is defined as the fraction of the radiated energy leaving surface i which strikes surface j.

Radiated energy from the arc strikes the back and sides of the box and is then reflected out towards the calorimeters. It is necessary to take multiple reflections into account, as these are not negligible. The inner surfaces behave as diffuse absorbers and reflectors with a reflectivity α. Incident radiation is reflected equally in all directions, as illustrated in Fig. 13.
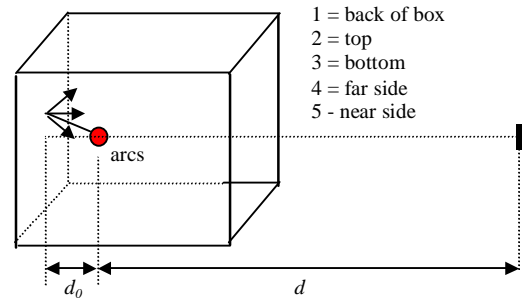

Figure 13. Box geometry for calculation of reflections

It is shown in [10] that the presence of the box can be taken into account by modifying equation (7) to

$$E_{max} = 84.61\, \{E_S + F_R(\alpha)\, W_{ARC}\}^{\,0.958}\, g^{\,0.284}\, V_{LL}^{\,-0.532} \qquad (8)$$

where the term $F_R(\alpha)\, W_{ARC}$ is an additional energy term due to single and multiple reflections from the back and sides of the box, and can be computed using radiative view factors which are calculated directly from the dimensions of the box. (The units of $F_R(\alpha)$ are mm^{-2}).

The only unknown is the reflectivity α. By varying α and computing the correlation between the predictions of (8) and the test data, the optimum value of α was found to be 0.56. In a typical case direct spherical radiation accounts for about 50% of the incident radiant energy. Fig. 14 shows a comparison between the incident energy density predicted by (8) and the measured mean maximum values for the entire IEEE data set.
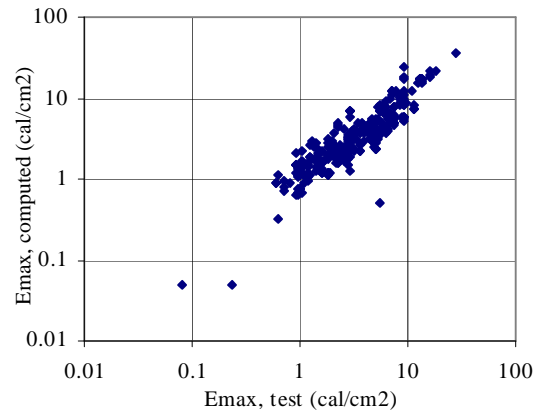

Figure 14. Time domain model prediction compared with test

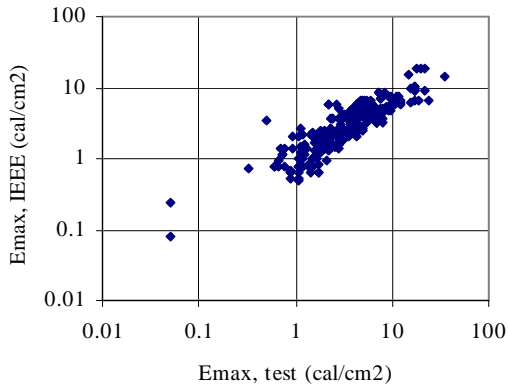Fig. 15 gives a similar comparison for the IEEE formula.

Figure 15. IEEE formula prediction compared with test

In this case the time-domain model gives a significantly better correlation ($r^2 = 0.856$) than the IEEE formula ($r^2 = 0.775$). Use of (8) also ensures that the incident energy density is always increased when the arcing fault is enclosed by a box.

VI. EFFECT OF CURRENT-LIMITING FUSES

A further advantage of the time domain approach is that it can be used to investigate interactions between the circuit, the arcing fault, and current-limiting fuses. The current-limiting fuse models used in this work were based on those described in [19], with some enhancements. They are summarized in the next two sections.

A. Prearcing model

During the prearcing time the fuse voltage is assumed to be zero, up to the time when the fuse melts. The instant of melting can be found by computing the evolution of the true r.m.s. current in each phase, and switching to the arcing state when the fuse's melting-time/current characteristic is crossed, as illustrated in Fig. 16.
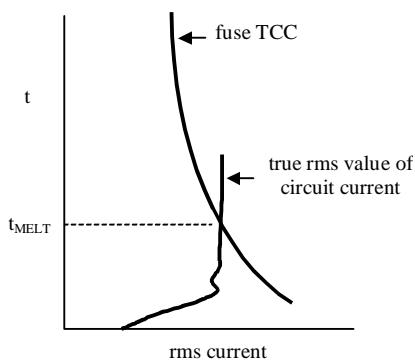

Figure 16. Computation of melting time

The fuse time-current characteristic is stored as a table which is dynamically fitted with cubic spline functions, and interpolation is used (as with all the models), to find the exact crossing point. For times shorter than the lowest tabulated value, the adiabatic melt I^2t is used.

The true r.m.s. (virtual) current in each phase is computed as

$$I_V = \sqrt{\frac{\int i^2 dt}{t}} \qquad (9)$$

B. Arcing models

Unlike free-burning arcs in air, the geometry of arcs in a sand-filled fuse is closely controlled by the surrounding quartz sand, and short-circuit faults can be modeled quite accurately. The models used here are fully described in [19] and include the effects of arc ignition in the fuse element notches, burnback of the elements, fusion of the sand and expansion of the arc cross-section, arc merging, and final arc extinction, each arc being modeled as a simple cylindrical channel. For each fuse design, details of the element construction and materials are needed, and the resulting models give very good agreement with oscillograms obtained from fuse type testing. The fuse models produce a further set of differential equations which have to be solved simultaneously with equation (4).

C. Typical results

Figs. 17-19 show the results of typical calculations for the interruption of a 50kA ungrounded arcing fault in a 600V 60Hz 3-phase system by three 800A class L fuses, closing at zero degrees of phase a. The other data used to obtain these results were in this section were:

p.f. = 0.1 $g = 32$ mm

$d_0 = 102$ mm $d = 457.2$ mm

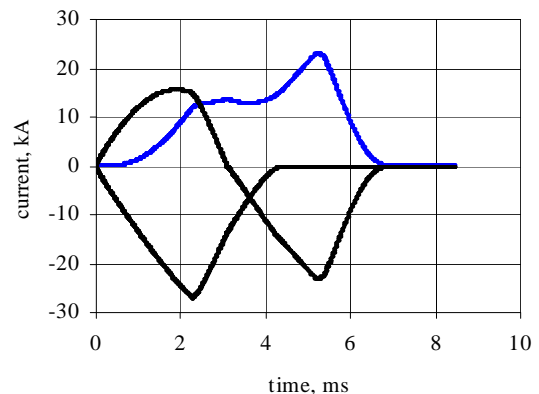and the box size was 508 x 508 x 508 mm.

Figure 17. Currents for arcing fault with fuses

Initially all three fuses are in the prearcing state, and the phase currents are lower than the available values because of the arcing fault voltages. In the case shown the fuse in phase c melts first and limits the current, the fuse arc voltage acting in series with the arcing fault voltage. The appearance of the phase c fuse arc voltage changes the rates-of rise of current in the other two phases. The phase b and phase a fuses melt just before the phase c fuse clears, and then the b and a fuses clear together against the line-to-line voltage.
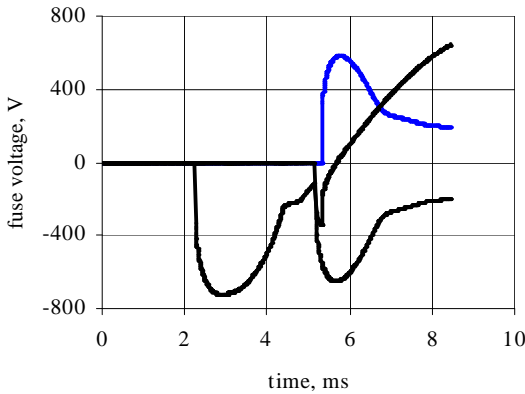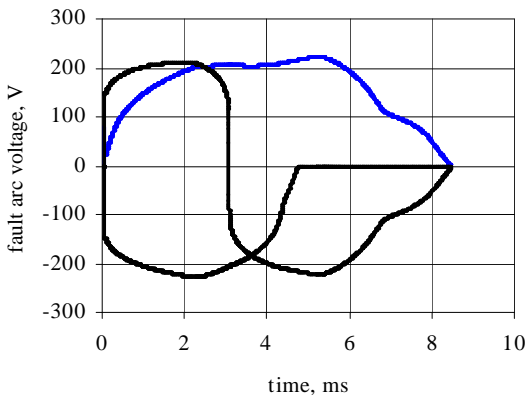
Figure 18.　Fuse arc voltages

Figure 19.　Arcing fault voltages

The possible sequences of events during clearing are very complicated, involving fuse melting and clearing in each phase, and interaction between the phases (if the fault is ungrounded). If a fuse just fails to melt within a particular half-cycle, the melting time jumps to a subsequent half-cycle. Sometimes all three fuses open, but in many cases only two fuses operate.

D.　Point-on-wave effects

The results are also affected by the point-on-wave at which the arcing fault begins. For 3-phase systems, all possible outcomes are covered if the closing angle θ (with respect to the voltage of phase a) is varied in the range $0 \leq \theta \leq 60°$.

A study of point-on-wave effects [10] has shown that below the fuse's current-limiting threshold current the incident energy density is not significantly affected by the closing angle, but within and above the threshold region the closing angle has a significant influence. After examining point-on-wave effects for several different fuse designs, and considering the additional variations which will be found in practice, due to the chaotic fault arc behavior, it is concluded that it is not possible to recommend a worst-case closing angle for arc-flash testing, in a similar way to that which is used for type testing of current-limiting fuses. The best method appears to be to use

random closing, but with several tests, to obtain a range of arc flash energy values.

E.　Arc flash characteristic

For a given set of data (equipment type and circuit parameters) it is useful to plot the arc flash energy density as a function of available current. Fig. 20 shows a typical theoretical characteristic computed using the time domain model for a set of three 1200A class L fuses. The upper curve is the maximum value (worst closing angle) and the lower curve is the minimum value (most favorable closing angle).
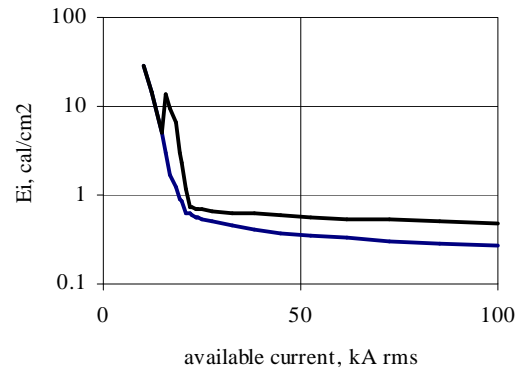

Figure 20.　Arc flash characteristic

Fig. 20 is similar to published test data [20] for 1200A class L fuses, although for slightly different test conditions. It shows that this fuse can limit the arc flash energy density to a level well below the critical value for a 2nd-degree burn (1.2 cal/cm^2), but only if the available bolted-fault current is high enough to cause operation in the current-limiting mode.

For these calculations it was assumed that the fault arcs could be represented by equation (6) with unchanged values of k, X and Y. However, some improvements are needed, because Stokes and Oppenlander [14] showed that for time durations of a few milliseconds, the arc does not move far from its starting location. During the first few cycles of arcing the arc length and voltage increase [9], so the fault arc geometry for very short times will be different from that which develops over a period of several cycles, giving a possibly significant change in fault arc voltage and incident energy.

VII.　CONCLUSIONS

A time-domain model of arc flash hazard has been developed. The ordinary differential equations for the 3-phase circuit and any current-limiting fuses are solved by 4th-order RK integration with automatic control of the time step.

The 3-phase arcing fault is represented as a star-connected set of non-linear resistors, and the their characteristics have been determined by least-squares fitting to the published IEEE dataset. The resulting arc characteristics are similar to those which have previously been measured for high-current single-phase and three-phase arcs in air.

For arcing faults in an open box, the focusing effect of the box is taken into account using radiation view factors to allow for multiple reflections of radiant heat.

The final model calculates the incident energy density due to the arc flash at a distance d for tests in the open or in a box of arbitrary dimensions, with a given electrical power system and interbus electrode gap. It gives good correlation with the IEEE 1584 test data and can also be used to study point-on-wave and other effects.

Whilst there is considerable scope for improving the arcing fault model used here, its interaction with the circuit is correctly represented, so that the anomalies of the IEEE 1584 equations are avoided.

Improvements which can be made to the model include a better representation of the reignition processes at current zero crossings and the dynamic growth of the fault arc lengths.

The model also illustrates the significant reduction in arc flash hazard which can be achieved if current-limiting fuse protection is used and the available fault current is high enough to cause the fuses to operate in their current-limiting region. Future testing may use Stokes and Sweeting's arrangement of the electrodes rather than that shown in Fig. 1. A modification of the incident energy model will be required in this case, as the heat transfer to the calorimeters will be increased due to the expanding plasma cloud. However the beneficial effects of current-limiting protection for high available currents will still apply.

REFERENCES

[1] National Electrical Code, 2002 Edition. National Fire Protection Association. NFPA 70.

[2] Standard for Electrical Safety Requirements for Employee Workplaces, NFPA 70E, draft 2004 Edition. National Fire Protection Association.

[3] Jones, R.A, and 9 other members of an IEEE-PCIC working group. "Staged Tests Increase Awareness of Arc-Flash Hazards in Electrical Equipment". IEEE Petroleum and Chemical Industry Conference Record, Sept 1997, pp 313-332.

[4] Lee, R.H. "The Other Electrical Hazard: Electric Arc Blast Burns". IEEE Transactions on Industry Applications, vol IA-18. No 3, May-June 1982, pp 246-251.

[5] Neal, T.E., Bingham, A.H. and Doughty, R.L. "Protective Clothing Guidelines for Electric Arc Exposure". IEEE Transactions on Industry Applications, vol 33, No 4, July/August 1997, pp 1043-1054.

[6] Doughty, R.L., Neal, T.E., and Floyd II, H.L. "Predicting Incident Energy to better manage the Electric Arc Hazard on 600V distribution systems". Proc.IEEE PCIC, Sept 1998, pp 329-346.

[7] Doughty, R.L., Neal, T.E., Dear, T.A. and Bingham, A.H. "Testing Update on Protective Clothing and Equipment for Electric Arc Exposure", IEEE Industry Applications Magazine, Jan-Feb 1999, pp 37-49.

[8] IEEE Guide for Performing Arc-Flash Hazard Calculations. IEEE Standard 1584, IEEE, September 2002.

[9] Stokes, A.D. and Sweeting, D.K. "Electric Arcing Burn Hazards", 7th International Conference on Electric Fuses and their Applications", Gdansk University of Technology, Poland, 8-10 Sept 2003, pp 215-222.

[10] Wilkins, R., Allison, M. and Lang, M. "Time-Domain Model of 3-phase Arc Flash Hazard", 7th International Conference on Electric Fuses and their Applications", Gdansk University of Technology, Poland, 8-10 Sept 2003, pp 223-231.

[11] Wilkins, R. "3-phase operation of current-limiting power fuses", 3rd Int Conf on Electric Fuses and their Applications, Eindhoven, 1987, pp 137-141.

[12] Fisher, L.E. "Resistance of low-voltage arcs". IEEE Transactions on Industry and General Applications, vol IGA-6, No 6, Nov-Dec 1970, pp 607-616.

[13] Ignatko, V.P. "Electric characteristics of AC open heavy-current arcs". 3rd International Symposium on Switching Arc Phenomena, TU Lodz, Poland, 1977, pp 98-102.

[14] Stokes, A.D. and Oppenlander, W.T. "Electric arcs in open air". J. Phys. D: Appl. Phys. vol 24, 1991, pp26-35.

[15] Paukert, J. "The arc voltage and the resistance of LV fault arcs". 7th International Symposium on Switching Arc Phenomena, TU Lodz, Poland, 1993, pp 49-51.

[16] Schau, H. and Stade, D. "Requirements to be met by protection and switching devices from the arcing protection point of view". Proceeding of 5th International Conference on Electric Fuses and their Applications, Technical University of Ilmenau, Germany, Sept 1995, pp 15-22.

[17] Gammon, T. and Matthews, J. "Instantaneous arcing-fault models developed for building system analysis". IEEE Transactions on Industry Applications, vol 37, No 1, 2001, pp197-203.

[18] Ozisik, M.N. "Heat Transfer", McGraw-Hill, 1985.

[19] Wilkins, R. "Standard Fuse Model for System Short-Circuit Studies." 8th International Symposium on Switching Arc Phenomena, TU Lodz, Poland, 1997, pp 163-166.

[20] Doughty, R.L., Neal, T.E., Macalady, T.L., and Saporita, V. "The use of Low-Voltage Current-Limiting Fuses to Reduce Arc Flash Energy." IEEE Transaction on Industry Applications, vol 36, no 6, November-December 2000, pp 1741-1749.